6-2019

In Search of Red *Noctiluca scintillans* Blooms in the East China Sea

Lin Qi
Xiamen University

Sheng-Fang Tsai
Taiwan Ocean University

Yanlong Chen
National Marine Environmental Monitoring Center

Chengfeng Le
Zhejiang University

Chuanmin Hu
University of South Florida, huc@usf.edu

AGU100 ADVANCING EARTH AND SPACE SCIENCE

Geophysical Research Letters

RESEARCH LETTER
10.1029/2019GL082667

In Search of Red *Noctiluca scintillans* Blooms in the East China Sea

Lin Qi[1,2], Sheng-Fang Tsai[3,4], Yanlong Chen[5], Chengfeng Le[6], and Chuanmin Hu[7]

[1]State Key Laboratory of Marine Environmental Science, Xiamen University, Xiamen, China, [2]Now at School of Marine Sciences, Sun Yat-Sen University (SYSU), Guangzhou, China, [3]Institute of Marine Environment and Ecology, National Taiwan Ocean University, Keelung City, Taiwan, [4]Center of Excellence for the Oceans, National Taiwan Ocean University, Keelung City, Taiwan, [5]National Marine Environmental Monitoring Center, Dalian, China, [6]Ocean College, Zhejiang University, Zhoushan, China, [7]College of Marine Science, University of South Florida, St Petersburg, FL, USA

Key Points:
- Red *Noctiluca scintillans* (*RNS*), which feeds on other algae, can be fingerprinted from satellite imagery
- The technique can be applied to nearly all existing sensors, regardless of number of bands or spatial resolution
- Long-term distributions of *RNS* blooms in the ECS provide unprecedented knowledge on their locations and environments

Supporting Information:
- Supporting Information S1

Correspondence to:
C. Hu,
huc@usf.edu

Citation:
Qi, L., Tsai, S.-F., Chen, Y., Le, C., & Hu, C. (2019). In search of red *Noctiluca scintillans* blooms in the East China Sea. *Geophysical Research Letters*, *46*, 5997–6004. https://doi.org/10.1029/2019GL082667

Received 2 MAR 2019
Accepted 26 APR 2019
Published online 12 JUN 2019

Abstract Red *Noctiluca scintillans* (*RNS*) is one of the major species causing red tides and bioluminescence, yet extremely difficult to track due to its ephemeral nature. Here, we show that *RNS* can be fingerprinted from satellite data due to its unique absorption and scattering properties. Retrospective analysis of Moderate Resolution Imaging Spectroradiometer data of 2000–2017 over the East China Sea reveals seasonal patterns and interannual changes as well as an increasing *RNS* bloom trend, all driven by hydrographical and biological factors and possibly by the construction of the Three Gorges Dam. Unlike earlier reports from field measurements, *RNS* blooms are found in both coastal and offshore waters of the ECS, to at least 126°E (> 330 km from the Yangtze River mouth). *RNS* blooms are also found in August and September where water temperature of 28–30 °C is well beyond the earlier reported range of 10–25 °C.

1. Introduction

The dinoflagellate *Noctiluca scintillans* (*NS* herein after) has been reported in all temperate, subtropical, and tropical coastal waters (Elbrächter & Qi, 1998; Harrison et al., 2011) from field surveys. There are two different forms of *NS*: red and green, and in this text for convenience they are called *RNS* and *GNS*, respectively. While they are both heterotrophic and feed on other phytoplankton and microzooplankton, only *GNS* contains a photosynthetic symbiont *Protoeuglena noctilucae* (Wang et al., 2016). The review by Harrison et al. (2011) shows that, while *GNS* is more restricted to a temperature range of 25–30 °C in Southeast Asia and the northern Arabian Sea (as well as adjacent ocean waters), *RNS* is found over a wide temperature range of 10–25 °C and high-salinity coastal regions all over the world. Indeed, *RNS* blooms have been reported in many such waters, for example, in the German Bight (Uhlig & Sahling, 1990), in the Seta Inland Sea of Japan (Tada et al., 2004), in the Sea of Mamara (Turkey) (Turkoglu, 2013), and in coastal waters of China (Tsai et al., 2018).

Studies of *RNS* are of particular importance for several reasons. First, it is one type of heterotrophic dinoflagellate causing red tides. Second, it can produce blue bioluminescence at night (often called "blue tears" in Southeast Asia), attracting tourists (Figure S1 in the supporting information). Finally, it is important to ocean ecology as it feeds on other phytoplankton and zooplankton. On the other hand, nearly all reports and studies of *RNS* and *GNS* are based on field and laboratory measurements, which are limited both spatially and temporally, thus making it difficult to explain bloom dynamics. One exception is perhaps in the northern Arabian Sea where satellite remote sensing has been used to characterize *GNS* blooms (do Rosário Gomes et al., 2014; others) with long-term trends attributed to eutrophication. Although *GNS* has distinctive absorption properties (much higher pigment absorption at 440 nm relative to 676 nm) from other commonly found phytoplankton groups (Figure S2a), it has been demonstrated, in the Arabian Sea, that it would be difficult to differentiate *GNS* from other phytoplankton from pure remote sensing spectroscopy (Thibodeau et al., 2014). It is only when the concentration is high enough near the surface that *GNS* blooms can be well distinguished from the surrounding waters in the satellite imagery. This is because they form patches or elongated slicks, where a reflectance peak in the green wavelength (555 nm) and a red-edge reflectance in the near infrared (NIR) can be clearly observed (Figure S2b). These reflectance features, on the other hand, are not unique to *GNS*, so unless some *a priori* knowledge is available, it is still difficult to fingerprint *GNS* from remote sensing spectroscopy.

In contrast, *RNS* has shown distinctive absorption and scattering properties (Figure S2c; Astoreca et al., 2005), thus making it distinguishable from other algae. This is because the enhanced absorption in the blue and enhanced scattering in the red and NIR lead to much higher reflectance in the red and NIR from *RNS*-rich waters than from surrounding waters (Figure S2d). Indeed, field and airborne measurements of *RNS* bloom patches in Belgium coastal waters confirmed this inference (Figure S2d; Van Mol et al., 2007), indicating that, at least in theory, *RNS* can be well distinguished from other algae in remote sensing imagery. The limitations, as discussed in Van Mol et al. (2007), come from whether the *RNS* concentration is high enough to result in a detectable signal and, more importantly, from whether the spatial resolution of remote sensing imagery is sufficient to detect the small *RNS* patches. In the study (Van Mol et al., 2007), the size of the *RNS* bloom patches or lines range from 0.5 to 50 m, making most of them difficult or even impossible to detect in medium-resolution imagery from, for example, the Moderate Resolution Imaging Spectroradiometer (MODIS; 250 m to 1 km resolution).

This is perhaps why, to date, our knowledge on *RNS* blooms is very limited due to a lack of synoptic and frequent observations. Therefore, given the reported global distribution of *RNS* (Harrison et al., 2011), its ecological and environmental importance, and the wide availability of medium-resolution satellite ocean color data to cover the global oceans every 1–2 days, one objective of this paper is to demonstrate how to remotely search for and fingerprint *RNS* blooms in optically complex waters, where other water constituents (e.g., suspended sediments, other types of algae, and colored dissolved organic matter) may also be abundant. A second objective is to study the long-term distributions of *RNS* blooms in the East China Sea (ECS, 27 to 35°N, 120°E to 126.5°E). ECS is selected because *RNS* blooms have been reported many times from field observations (Tang et al., 2006; Tsai et al., 2018; Tseng et al., 2011; Xu, 2009). On the other hand, located downstream of the Yangtze River, the ECS is biologically and ecologically complex, where blooms of diatoms, dinoflagellate of *Prorocentrum donghaiense* (Lou & Hu, 2014; Shang et al., 2014; Tang et al., 2006; Tao et al., 2017), *Ulva* macroalgae (Hu, Li, et al., 2010; Qi et al., 2016), and *Sargassum* macroalgae (Qi et al., 2017) have frequently occurred. Thus, we hope to use this study as a proof of concept to facilitate studies of *RNS* in many other regions with similar optical and biological complexities.

2. Materials and Methods

2.1. Satellite Imagery and Data Products

Three types of remote sensors are used here (Table S1). One type is multiband medium-resolution (250 m to 1 km) sensors such as MODIS and Geostationary Ocean Color Imager (GOCI); a second type is multiband high-resolution (8–30 m) sensors such as Gao-Fen-1 (GF-1) and Operational Land Imager (OLI); the last type is the Hyperspectral Imager for the Coastal Ocean (HICO, 90 m). While MODIS (both Terra and Aqua) and HICO are used systematically to search for *RNS*, other sensors are used to show their capacity only.

Based on the reported optical properties of *RNS* (Astoreca et al., 2005; Van Mol et al., 2007), image pixels rich in *RNS* should be highly reflective in the red and NIR wavelengths (Figure S2d) because of strong blue-green absorption (Figure S2c). Such elevated reflectance is known to cause atmospheric correction failure (Gordon & Wang, 1994; Stumpf et al., 2003). Therefore, only a partial atmospheric correction was applied to low-level data to generate Rayleigh-corrected reflectance ($R_{rc}(\lambda)$, dimensionless) using the National Aeronautics and Space Administration's SeaDAS software (version 7.4; MODIS and HICO) or software developed in house that utilized the Rayleigh reflectance lookup table embedded in SeaDAS (GF-1). The only exception was OLI, where Acolite software (Vanhellemont & Ruddick, 2015) was used to generate $R_{rc}(\lambda)$. While the band wavelengths, calibrations, and processing steps in SeaDAS and Acolite) may be different for these sensors (Table S1), such differences will have negligible impacts on sensor-specific R_{rc} spectra when nearby water pixels are used as the reference (see below).

Because standard ocean color data products cannot be used, two forms of nonstandard imagery products were generated from $R_{rc}(\lambda)$ in order to search for *RNS*:

1. Natural color Red-Green-Blue (RGB) imagery. For MODIS, the RGB bands are 645, 555, and 469 nm, respectively. For other sensors, these bands are adjusted according to their band availability.
2. False color RGB imagery, where a NIR band (859 nm for MODIS) is used to replace the green band (555 nm for MODIS) in the RGB imagery.

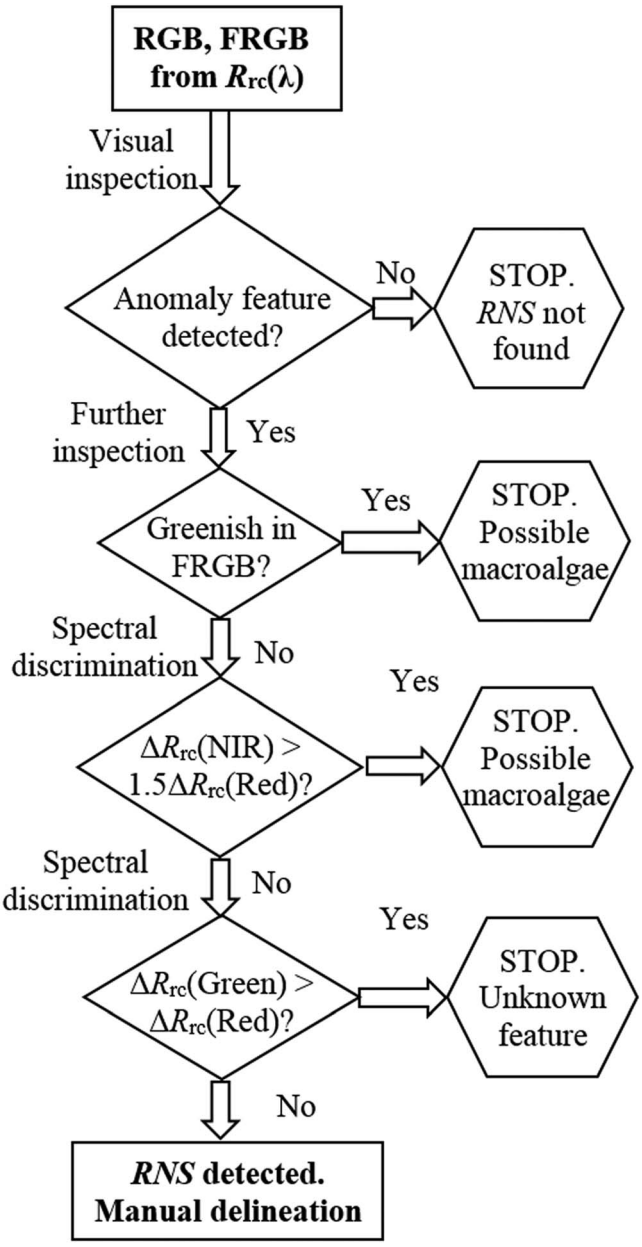

Figure 1. Flowchart showing how to detect *RNS* features through visual inspection of RGB/FRGB imagery and through spectral discrimination of visually identified features. Here ΔR_{rc} represents R_{rc} difference of the feature pixel against nearby water pixels. NIR can be ~750 nm (or ~860 nm if 750 nm is not available), Red can be ~640 or ~660 nm, and Green can be ~550 nm. *RNS* = Red *Noctiluca scintillans*; RGB = Red-Green-Blue; NIR = near infrared.

For MODIS, 2,052 five-minute data granules covering the ECS between 2000 and 2017 for the months of April–August were processed. Of these granules, only half of them (996) were found to have greater than one third of the pixels being cloud free. For HICO, all available 41 data granules covering the ECS from September 2009 to September 2014 were processed to generate $R_{rc}(\lambda)$. For GOCI and other sensors, selected data granules were processed to test their capacity in detecting RNS using the same rules established for MODIS.

Once an image feature was visually identified from RGB or FRGB imagery, spectral analysis was used to examine the spectral shape. Because *RNS* features may be much smaller than the pixel size, the analysis was performed over the $R_{rc}(\lambda)$ difference against nearby water, which was then compared against known spectra of floating algae. The rules of searching and identifying *RNS* features were then established (Figure 1).

Such established rules were applied to the entire MODIS time series. Ultimately, an objective method to automatically detect and delineate *RNS* features is preferred (while masking clouds and cloud shadows). However, because of the frequent nonoptimal observation conditions (see Figure S2 of Qi et al., 2017), for this proof-of-concept study, the *RNS* features were manually delineated to roughly outline their boundaries. For each calendar month, all such outlined boundaries were merged to derive the aggregated monthly coverage of *RNS* features, from which an annual summary was obtained for each year between 2000 and 2017.

3. Results and Discussion

While many full-resolution images are presented in the supporting information (Figures S3–S6), several examples are given below to show the concept of detecting *RNS* blooms using multiband remote sensing data, where the stepwise rules are illustrated in the flow-chart of Figure 1.

Even though *RNS* can float on the surface of the ocean due to its density being lower than water (Harvey, 1917), the difficulty of finding *RNS* blooms is demonstrated in Figure 2. Of all 41 HICO images between 2009 and 2014, only one image (Figure 2b) shows some yellowish-brownish slicks near the Yangtze River mouth (Figure 2d). These slicks are difficult to visually identify even by a human analyst, not to mention nearly impossible with automatic digital detection. However, spectral analysis of several randomly selected pixels from these slicks (annotated as 1, 2, and 3 in Figure 2d) indicates near-identical spectral shapes as compared with those from field-measured *RNS* blooms (Figures 2f and S1d). They all show sharp reflectance increases from ~510 to ~600 nm, a specific result of *RNS* absorption and scattering (Figure S1c; Astoreca et al., 2005).

The magnitudes of the HICO spectra are different—a result of different *RNS* proportion within a pixel. For example, assuming a 100% *RNS* portion has reflectance of ~0.17 in the NIR (Figure S2d), the three pixels in Figure 2f represent approximately 30%, 17%, and 8% of partial *RNS* coverage within a 90-m HICO pixel. Likewise, the two pixels in Figure 2 g represent about 10% and 8% of partial *RNS* coverage within a 250-m MODIS pixel. Note that because of the larger pixel size, the MODIS image appears more blurred than HICO in revealing the *RNS* slicks.

Many MODIS images show features that can be determined to be *RNS* through image inspection and spectral analysis following the stepwise rules established in Figure 1, where Figure 3 presents an example. Figure 3a shows a MODIS FRGB image on 18 May 2017, where a small area is enlarged in Figure 3b. Surface algae slicks of yellowish/brownish and greenish colors, respectively, can be clearly visualized. The

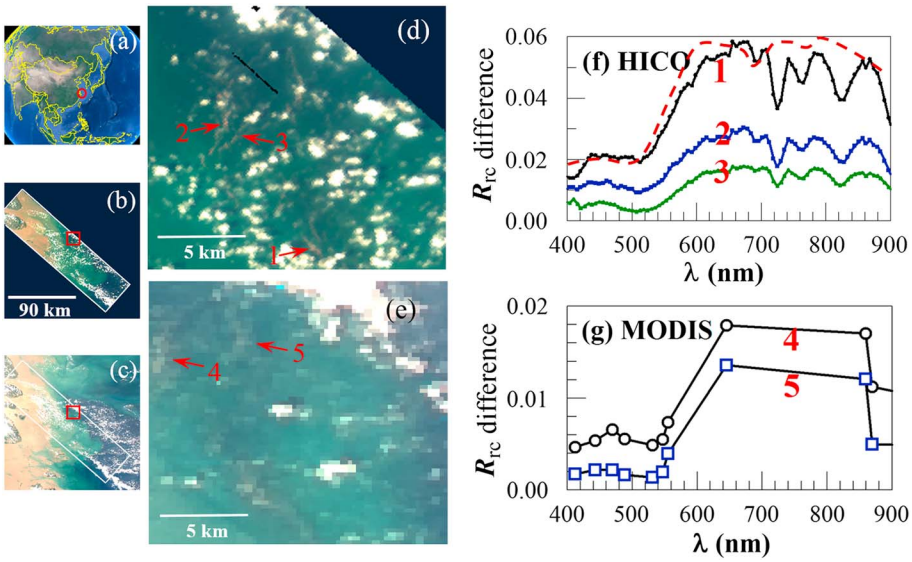

Figure 2. Fingerprinting Red *Noctiluca scintillans* blooms through remote sensing spectroscopy. (a) Google Earth map shows approximate location of the HICO Red-Green-Blue image (b) and MODIS RGB image (c) captured on 9 September 2013 06:08 and 04:45 GMT, respectively, covering the region between 30.25–32°N and 121.75–123.5°E. The white rectangle in (c) corresponds to the HICO coverage in (b). A small region, outlined by the red square in (b) and (c) (31.15–31.30°N, 122.58–122.75°E), is enlarged in (d) and (e), respectively, where some weak image slicks of yellowish-brownish colors can be visualized. Some pixels (annotated by 1–5) are selected randomly for spectroscopic diagnosis in (f) and (g) for HICO and MODIS, respectively. For reference, a typical water-leaving reflectance spectrum from a red *NS* bloom off Belgium (Van Mol et al., 2007) is shown in (f) (red dashed line). HICO = Hyperspectral Imager for the Coastal Ocean; MODIS = Moderate Resolution Imaging Spectroradiometer.

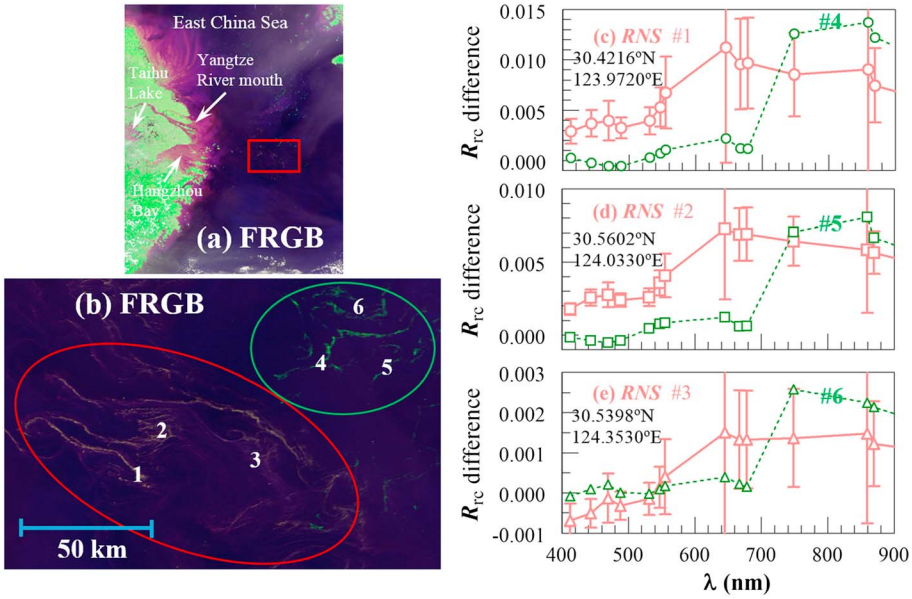

Figure 3. Demonstration of detecting and fingerprinting a *RNS* bloom in the ECS (27°N to 35°N, 120°E to 126.5°E) through Moderate Resolution Imaging Spectroradiometer remote sensing spectroscopy. (a) Moderate Resolution Imaging Spectroradiometer FRGB image on 18 May 2017 shows the study region. The area outlined in the rectangle (30.1–31.1°N, 123.5–125°E) is enlarged in (b), where surface slicks of yellowish/brownish and greenish colors can be visualized. Several randomly selected pixels (#1 to #6, location annotated) from both types of features are diagnosed for their R_{rc} difference spectra, which are shown in (c)–(e). Each R_{rc} difference spectrum is an average of 3 km × 3 km centered at the pixel of interest, referenced against nearby water pixels. Vertical bars represent standard deviations, where land bands (645, 859, 469, and 555 nm) show higher standard deviations than other bands because of their higher spatial resolution and patchiness of the algae features. *RNS* = Red *Noctiluca scintillans*; RGB = Red-Green-Blue.

latter have been reported to be *Sargassum horneri* (Qi et al., 2017), while the former are determined to be *RNS* (Figures 3c–3e). Specifically, R_{rc} difference at >555 nm is significantly higher than in shorter wavelengths, with the maximum at 645 nm regardless of the absolute magnitude (0.0014–0.011 at 645 nm). This spectral characteristic is nearly identical to those reported from field measurements of *RNS* (Figure S2d and dashed line in Figure 2f). Therefore, from a pure spectroscopy perspective, these yellowish/brownish slicks can be inferred to be *RNS*. In contrast, the pixels from the greenish slicks show typical spectral shapes of *Sargassum* (Figures 3c–3e) that are easily distinguishable from those of *RNS*. Note that such a spectral discrimination is performed over the R_{rc} difference spectra rather than R_{rc} spectra, as the latter are often "smeared" by water if *RNS* only occupies a small portion of a pixel (Figure S7).

From results similar to those in Figure 3, the following stepwise rules were established to search for *RNS* from satellite imagery (Figure 1):

1. While both *RNS* and *Sargassum* can be visualized in FRGB imagery, only *RNS* can be revealed clearly in RGB imagery.
2. *RNS* and *Sargassum* (and other macroalgae such as *Ulva*) show different colors in FRGB imagery, with the latter appearing greenish.
3. To qualify for a *RNS*-containing pixel, ΔR_{rc}(NIR) cannot be more than 1.5ΔR_{rc}(Red), and ΔR_{rc} (Green) cannot be more than ΔR_{rc} (Red). Here ΔRrc represents Rrc difference between the pixel of interest and nearby water pixels.

This stepwise method (Figure 1) was applied to all MODIS imagery between 2000 and 2017 for the months of April–August. Figure 4 shows a summary of the annual occurrences of *RNS* features and their approximate locations.

The annual sequence shows clear interannual variations in *RNS* bloom location, size, distribution, and occurrence months. For example, in 2002, there was not a single image showing *RNS* features, but in 2017, there were many images in months between April and August that showed *RNS* features. Unlike those reported earlier from field-based observations, although most of the *RNS* features were found near the Yangtze estuary, off Hangzhou Bay, or along the coast of Zhejiang Province, many *RNS* features were found in offshore waters to 126°E (>330 km from Hangzhou Bay). Furthermore, although there is substantial interannual variability, there appears to be an increasing trend in recent years in terms of the RNS bloom occurrence size and duration, especially between 2013 and 2017, with 2017 being the maximum year.

These findings provide a more complete picture (than any previous study) on the seasonality and interannual changes of *RNS* blooms (e.g., fewer blooms before 2003). The seasonality of *RNS* bloom formations has been proposed to be regulated by a variety of hydrographical and biological factors (Miyaguchi et al., 2006). Availability of phytoplankton as prey is one of the important factors (Elbrächter & Qi, 1998). The Yangtze River discharges 924.8×10^9 m^3/year freshwater annually into the ECS, contributing nutrient flux of inorganic nitrogen, phosphate, and silicate (Duan et al., 2000; Liu et al., 2003; Tian et al., 1993). The construction of the Three Gorges Dam began in 1994, with the first filling stage of the reservoir completed in June 2003, and full-scale operations began in 2009. Gong et al. (2006) found that the Si:N ratio in the affected Yangtze River region changed from 1.5 in 1998 to 0.4 in 2004 and that primary production had declined by 86% between 1998 and 2003. Hence, the inconstant input of freshwater during the first filling stage of the reservoir might be the main cause of the lower occurrence of *RNS* blooms, especially during years 2001–2003. Accumulation of buoyant cells caused by convergence of surface seawater is suggested as another factor leading to *NS* blooms or aggregations (Elbrächter & Qi, 1998). With the development of a subtropical summer monsoon climate in the ECS in mid-May, the southwest wind is strengthened with time, causing the distribution of *RNS* to shift northward in the same year. Additionally, the increased occurrence of *RNS* after 2013 indicates a rich food supply for *RNS* in recent years (Sriwoon et al., 2008).

Year 2017 is an exceptional year for a prolonged and extensive *RNS* bloom. Figure 4 shows that *RNS* slicks first appeared along the Zhejiang coast in MODIS imagery in April (14 April 2017). Then, by mid-May, *RNS* slicks appeared extensively from the Zhejiang coast to the Yangtze estuary, as well as in offshore waters. By June 2017, *RNS* slicks were only found near the Yangtze estuary and Hangzhou Bay; this lasted until July 2017. In August 2017 only some small *RNS* slicks were found in MODIS imagery. The *RNS* bloom event lasted for at least 3 months between mid-April and mid-July 2017. While the exact reason of the

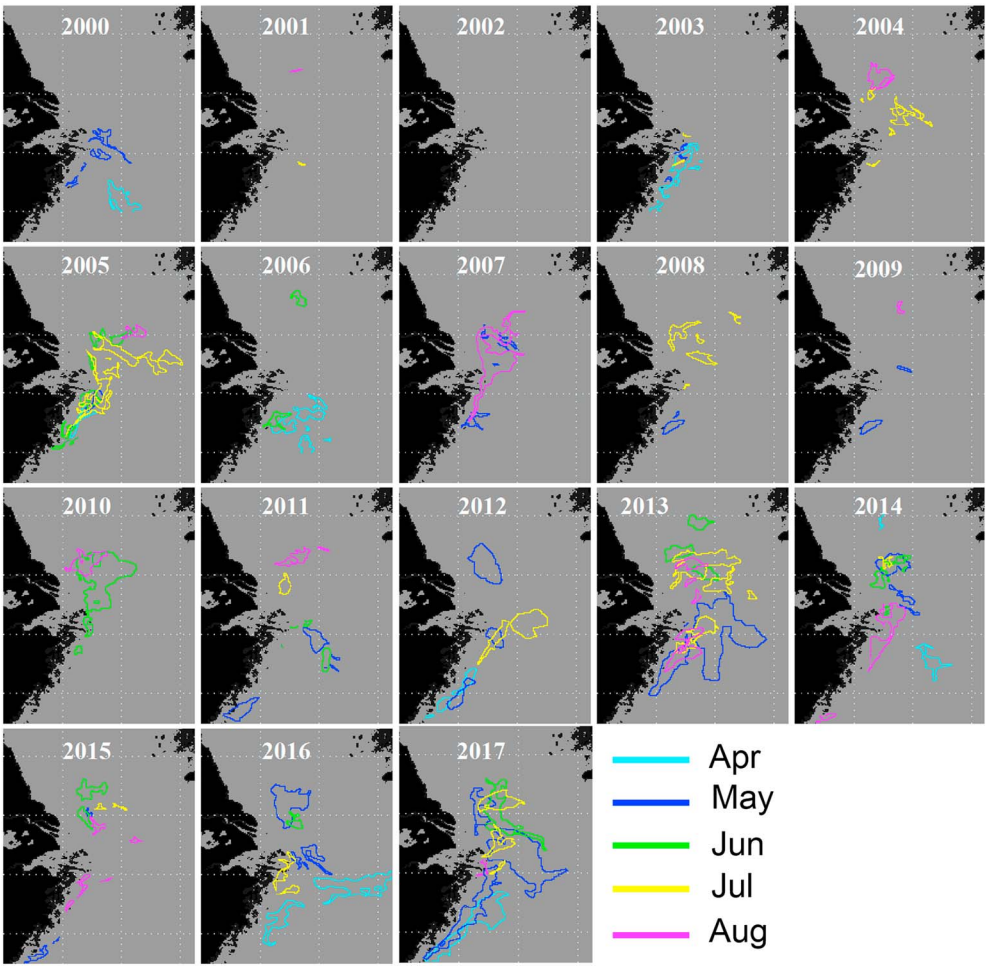

Figure 4. Monthly distributions of approximate *RNS* feature locations for April–August between 2000 and 2017 in the ECS (27°N – 35°N, 120°E – 126.5°E), determined from Moderate Resolution Imaging Spectroradiometer imagery and spectral analysis. Certain (or all) colors may not appear in an annual summary image (e.g., 2002), meaning that no *RNS* features were found in those months.

prolonged and extensive *RNS* bloom in 2017 has yet to be investigated, it is speculated that the unusual red tide blooms of *Prorocentrum donghaiense*, as indicated by the anomalous MODIS nFLH images (see https://optics.marine.usf.edu/cgi-bin/optics_data?roi=YS_ECS&Date=5/18/2017&Pass=A0515), may provide sufficient food to feed *RNS*. As speculated in Qi et al. (2017) to explain the record-high *Sargassum* bloom in the ECS in 2017, recent eutrophication, higher-than-usual temperature, and increased light availability could be other reasons behind the 2017 *RNS* bloom.

Satellite images from GOCI (500 m), OLI (30 m), and GF-1 (8 m) all show the same capacity to detect and differentiate *RNS* features when using the method developed here (see Figures S3–S6). This is despite the differences in their spectral bands, resolutions, and calibrations. The success is attributed to the use of R_{rc} difference rather than the absolute R_{rc}. The difference not only compensates for potential calibration errors (because the errors are the same between the *RNS* and water pixels) and inconsistencies in band wavelengths but also more importantly reveals the unique spectral shapes of *RNS* that are otherwise extremely difficult to differentiate, especially when *RNS* only occupies a small portion of a pixel (Figure S7). On the other hand, although OLI and GF-1 can detect much smaller *RNS* features than those medium-resolution sensors, their scarce coverage makes it impossible to provide a full picture as shown in Figure 4 by MODIS. In any case, the ability to detect *RNS* features from satellite imagery can provide guidance for future field surveys in response to *RNS* bloom events. In turn, field measurements can provide direct validation to satellite observations in addition to detailed information on the *RNS* composition and their living environment. Currently, due to lack of such a guidance, the only field survey that was concurrent

and collocated with satellite detected *RNS* was on 2 May 2016 around 26.7906°N 120.4484°E off the Zhejiang coast. The survey encountered high-concentration *RNS* patches through visual sightings, confirming the OLI observations.

While the capacity of satellite remote sensing in detecting *RNS* blooms is fully demonstrated here, three limitations still exist. The first comes from the data coverage and sensor sensitivity (Hu et al., 2015). Regardless of cloud cover, cloud shadow, sun glint, and other nonoptimal observing conditions, only large-swath medium-resolution sensors such as MODIS can provide near-daily coverage, yet the large pixel size is known to miss small patches of *RNS*. For this reason, *RNS* detection results simply represent those *observable* by the sensor. The second is that it is currently difficult to automate the detection and delineation process due to frequent nonoptimal observing conditions. The third and also the most significant limitation is that the current detection is only applicable to near-surface high concentrations of *RNS*, but *RNS* cells may be well mixed through the water column, presenting a significant challenge in detection and quantification. One major reason behind this limitation is the lack of measurements of *RNS* bio-optical properties (absorption, scattering, and scattering phase function); the works by Astoreca et al. (2005) and Van Mol et al. (2007) are perhaps the only exceptions that show preliminary data. Clearly, future efforts of remote quantification of *RNS* will require coordinated efforts in field and laboratory measurements as well as development of inversion algorithms (e.g., Shang et al., 2014; Tao et al., 2017).

In summary, through image inspection and spectral analysis, this proof-of-concept study demonstrates that it is possible to detect *RNS* blooms through satellite remote sensing using either medium- or high-resolution sensors. The detection is based on the fact that *RNS* has strong absorption in the blue-green wavelengths and strong scattering in all wavelengths, which lead to elevated reflectance in all red and NIR wavelengths. This spectral characteristic makes *RNS* well distinguishable from other types of floating algae (e.g., *Sargassum*, *Ulva*) and also makes *RNS* features distinguishable during image and spectral inspection. Correspondingly, the stepwise rules (Figure 1) can be used to detect *RNS* features from satellite imagery. This is similar to the spectral analysis used to identify a *Mesodinium rubrum* bloom using HICO observations (Dierssen et al., 2015) and detecting *Trichodesmium* blooms using multiband Sea-viewing Wide Field-of-view Sensor or MODIS observations (Hu, Cannizzaro, et al., 2010; Subramaniam et al., 2002). With the ongoing sensors and the projected hyperspectral PACE (Plankton, Aerosol, Cloud, and ocean Ecosystem) mission in the near future, the study here is expected to encourage more research on *RNS* bio-optical properties and their ecological behaviors in various tropical and subtropical waters where *RNS* blooms have been reported.

Acknowledgments
This work was supported by the National Natural Science Foundation of China (41806208, 41431176), China Postdoctoral Science Foundation (2017M610393 and 2018T110645; Qi), and the U.S. National Oceanic and Atmospheric Administration (NA15OAR4320064) and the National Aeronautics and Space Administration (NNX14AL98G; Hu). We thank NASA, NOAA, USGS (United States Geological Survey), and KORDI for providing satellite data. We also thank Prof. Dazhi Wang (Xiamen University) for the useful discussions on RNS occurrence in the ECS. The extensive comments from an anonymous reviewer are appreciated. All satellite imagery and data are available on the Web (https://optics.marine.usf.edu/cgi-bin/optics_data?roi=ECS&current=1).

References

Astoreca, R., Rousseau, V., Ruddick, K., Van Mol, B., Parent, J.-Y., & Lancelot, C. (2005). Optical properties of algal blooms in an eutrophicated coastal area and its relevance to remote sensing. In R. J. Frouin, M. Babin, & S. Sathyendranath (Eds.), *Remote Sensing of the Coastal Oceanic Environment*, *Proc. SPIE*, (Vol. 5885, pp. 245–255).

Dierssen, H. M., Chlus, A., & Russell, B. (2015). Space station image captures a red tide ciliate bloom at high spectral and spatial resolution. *PNAS*, *112*(48), 14783–14787. https://doi.org/10.1073/pnas.1512538112

do Rosário Gomes, H., Goes, J. I., Matondkar, S., Buskey, E. J., Basu, S., Parab, S., & Thoppil, P. (2014). Massive outbreaks of Noctiluca scintillans blooms in the Arabian Sea due to spread of hypoxia. *Nature Communications*, *5*(1), 4862. https://doi.org/10.1038/ncomms5862

Duan, S., Zhang, S., & Huang, H. (2000). Transport of dissolved inorganic nitrogen from the major rivers to estuaries in China. *Nutrient Cycling in Agroecosystems*, *57*, 13–22.

Elbrächter, M., & Qi, Z. (1998). Aspects of Noctiluca (Dinophyceae) population dynamics. In D. M. Anderson, A. D. Cembella, & G. M. Hallegraeff (Eds.), *Physiological ecology of harmful algal blooms*, (pp. 315–335). Berlin, Heidelberg: Springer.

Gong, G. C., Chang, J., Chiang, K. P., Hsiung, T. M., Hung, C. C., Duan, S. W., & Codispoti, L. (2006). Reduction of primary production and changing of nutrient ratio in the East China Sea: Effect of the Three Gorges Dam? *Geophysical Research Letters*, *33*, L07610. https://doi.org/10.1029/2006GL025800

Gordon, H. R., & Wang, M. (1994). Retrieval of water-leaving radiance and aerosol optical thickness over the oceans with SeaWiFS: A preliminary algorithm. *Applied Optics*, *33*(3), 443–452. https://doi.org/10.1364/AO.33.000443

Harrison, P. J., Furuya, K., Glibert, P. M., Xu, J., Liu, H., Yin, K., et al. (2011). Geographical distribution of red and green Noctiluca scintillans. *Chinese Journal of Oceanology and Limnology*, *29*, 807–831.

Harvey, E. B. (1917). A physiological study of Noctiluca, with special reference to light production, anaesthesia and specific gravity. *Proceedings of the National Academy of Sciences*, *3*, 15–16.

Hu, C., Cannizzaro, J., Carder, K. L., Muller-Karger, F. E., & Hardy, R. (2010). Remote detection of Trichodesmium blooms in optically complex coastal waters: Examples with MODIS full-spectral data. *Remote Sensing of Environment*, *114*(9), 2048–2058. https://doi.org/10.1016/j.rse.2010.04.011

Hu, C., Feng, L., Hardy, R. F., & Hochberg, E. J. (2015). Spectral and spatial requirements of remote measurements of pelagic *Sargassum* macroalgae. *Remote Sensing of Environment*, *167*, 229–246. https://doi.org/10.1016/j.rse.2015.05.022

Hu, C., Li, D., Chen, C., Ge, J., Muller-Karger, F. E., Liu, J., et al. (2010). On the recurrent Ulva prolifera blooms in the Yellow Sea and East China Sea. *Journal of Geophysical Research*, *115*, C05017. https://doi.org/10.1029/2009JC005561

Liu, S. M., Zhang, J., Chen, H., Wu, Y., Xiong, H., & Zhang, Z. J. B. (2003). Nutrients in the Changjiang and its tributaries. *Biogeochemistry*, *62*(1), 1–18. https://doi.org/10.1023/A:1021162214304

Lou, X., & Hu, C. (2014). Diurnal changes of a harmful algal bloom in the East China Sea: Observations from GOCI. *Remote Sensing of Environment*, *140*, 562–572. https://doi.org/10.1016/j.rse.2013.09.031

Miyaguchi, H., Fujiki, T., Kikuchi, T., Kuwahara, V. S., & Toda, T. (2006). Relationship between the bloom of Noctiluca scintillans and environmental factors in the coastal waters of Sagami Bay, Japan. *Journal of Plankton Research*, *28*(3), 313–324. https://doi.org/10.1093/plankt/fbi127

Qi, L., Hu, C., Xing, Q., & Shang, S. (2016). Long-term trend of *Ulva prolifera* blooms in the western Yellow Sea. *Harmful Algae*, *58*, 35–44. https://doi.org/10.1016/j.hal.2016.07.004

Qi, L., Hu, C., Wang, M., Shang, S., & Wilson, C. (2017). Floating algae blooms in the East China Sea. *Geophysical Research Letters*, *44*, 11,501–11,509. https://doi.org/10.1002/2017GL075525

Shang, S., Wu, J., Huang, B., Lin, G., Lee, Z., Liu, J., & Shang, S. (2014). A new approach to discriminate dinoflagellate from diatom blooms from space in the East China Sea. *Journal of Geophysical Research: Oceans*, *119*, 4653–4668. https://doi.org/10.1002/2014JC009876

Sriwoon, R., Pholpunthin, P., Lirdwitayaprasit, T., Kishino, M., & Furuya, K. (2008). Population dynamics of green Noctiluca scintillans (Dinophyceae) associated with the monsoon cycle in the upper Gulf of Thailand. *Journal of Phycology*, *44*(3), 605–615. https://doi.org/10.1111/j.1529-8817.2008.00516.x

Stumpf, R., Arnone, R., Gould, R., Martinolich, P., & Ransibrahmanakul, V. (2003). A partially coupled ocean-atmosphere model for retrieval of water-leaving radiance from SeaWiFS in coastal waters. *NASA Tech. Memo*, 206892, 51-59

Subramaniam, A., Brown, C. W., Hood, R. R., Carpenter, E. J., & Capone, D. G. (2002). Detecting Trichodesmium blooms in SeaWiFS imagery. *Deep-Sea Research Part II*, *49*, 107–121.

Tada, K., Pithakpol, S., & Montani, S. (2004). Seasonal variation in the abundance of Noctiluca scintillans in the Seto Inland Sea, Japan. *Plankton Biology and Ecology*, *51*, 7–14.

Tang, D. L., Di, B. P., Wei, G., Ni, I. H., Oh, I. S., & Wang, S. F. (2006). Spatial, seasonal and species variations of harmful algal blooms in the South Yellow Sea and East China Sea. *Hydrobiologia*, *568*(1), 245–253. https://doi.org/10.1007/s10750-006-0108-1

Tao, B., Mao, Z., Lei, H., Pan, D., Bai, Y., Zhu, Q., & Zhang, Z. (2017). A semianalytical MERIS green-red band algorithm for identifying phytoplankton bloom types in the East China Sea. *Journal of Geophysical Research: Oceans*, *122*, 1772–1788. https://doi.org/10.1002/2016JC012368

Thibodeau, P. S., Roesler, C. S., Drapeau, S. L., Prabhu Matondkar, S., Goes, J. I., & Werdell, P. J. (2014). Locating Noctiluca miliaris in the Arabian Sea: An optical proxy approach. *Limnology and Oceanography*, *59*(6), 2042–2056. https://doi.org/10.4319/lo.2014.59.6.2042

Tian, R., Hu, F., & Martin, J. (1993). Summer nutrient fronts in the Changjiang (Yantze River) estuary. *Estuarine, Coastal and Shelf Science*, *37*(1), 27–41. https://doi.org/10.1006/ecss.1993.1039

Tsai, S.-F., Wu, L.-Y., Chou, W.-C., & Chiang, K.-P. (2018). The dynamics of a dominant dinoflagellate, Noctiluca scintillans, in the sub-tropical coastal waters of the Matsu archipelago. *Marine Pollution Bulletin*, *127*, 553–558. https://doi.org/10.1016/j.marpolbul.2017.12.041

Tseng, L.-C., Kumar, R., Chen, Q.-C., & Hwang, J.-S. (2011). Summer distribution of Noctiluca scintillans and mesozooplankton in the Western and Southern East China Sea prior to the Three Gorges Dam operation. *Hydrobiologia*, *666*(1), 239–256. https://doi.org/10.1007/s10750-010-0587-y

Turkoglu, M. (2013). Red tides of the dinoflagellate Noctiluca scintillans associated with eutrophication in the Sea of Marmara (the Dardanelles, Turkey). *Oceanologia et Limnologia Sinica/Hai Yang Yu Hu Chao*, *55*, 709–732.

Uhlig, G., & Sahling, G. (1990). Long-term studies on Noctiluca scintillans in the German Bight population dynamics and red tide phenomena 1968–1988. *Netherlands Journal of Sea Research*, *25*(1-2), 101–112. https://doi.org/10.1016/0077-7579(90)90012-6

Van Mol, B., Ruddick, K., Astoreca, R., Park, Y., & Nechad, B. (2007). Optical detection of a Noctiluca scintillans bloom. *EARSeL eProceedings*, 6, 130

Vanhellemont, Q., & Ruddick, K. (2015). Advantages of high quality SWIR bands for ocean colour processing: Examples from Landsat-8. *Remote Sensing of Environment*, *161*, 89–106. https://doi.org/10.1016/j.rse.2015.02.007

Wang, L., Lin, X., Goes, J. I., & Lin, S. (2016). Phylogenetic analyses of three genes of Pedinomonas noctilucae, the green endosymbiont of the marine dinoflagellate Noctiluca scintillans, reveal its affiliation to the order Marsupiomonadales (Chlorophyta, Pedinophyceae) under the reinstated name Protoeuglena noctilucae. *Protist*, *167*(2), 205–216. https://doi.org/10.1016/j.protis.2016.02.005

Xu, Z. (2009). The inter-annual variations in Noctiluca scintillans abundance and eutrophication in Changjiang estuary. *Oceanologia et Limnologia Sinica*, *40*, 793–798.